

Analogue of Charge Conjugation in the Optical Spin Hall Effect

Yuquan Zhou,¹ Haochen Wang,¹ Song Luo,¹ Hang Zhou,¹ Junhui Cao,^{3,4} T.-S. Zeng,¹ Yunmei Li,¹ Alexey Kavokin^{1,2,3,4,5,6}, Long Zhang,^{1,2,*} and Zhanghai Chen^{1,†}

¹Department of physics, College of Physical Science and Technology, Xiamen University, Xiamen 361005, China

²State Key Laboratory of Surface Physics and Department of Physics, Fudan University, Shanghai 200433, China

³Key Laboratory for Quantum Materials of Zhejiang Province, School of Science, Westlake University, 18 Shilongshan Road, Hangzhou, Zhejiang Province 310024, China

⁴Institute of Natural Sciences, Westlake Institute for Advanced Study, 18 Shilongshan Road, Hangzhou, Zhejiang Province 310024, China

⁵Spin Optics Laboratory, St-Petersburg State University, 1 Ulyanovskaya, St Petersburg 198504, Russia

⁶School of Physics and Astronomy, University of Southampton, Highfield, Southampton SO17 1BJ, United Kingdom

(Received 25 April 2023; revised 30 June 2023; accepted 21 July 2023; published 10 August 2023)

The optical spin Hall effect, as an optical analogue of spin-orbit coupling of fermionic electrons, has attracted increasing interest in fundamental physics and nanophotonic applications. In addition to spin, charge of particles, as the other degree of freedom, plays a significant role in spin-orbit interaction as well. However, the optical counterpart of charge conjugation has been absent due to the charge-free nature of photons. Here, in a one-dimensional photonic crystal, we report reversible optical spin currents from the opposite band edges of the photonic band gap, which can provide an optical analogue of charge conjugation in spin-orbit coupling. The effective magnetic field acting on the photons is controlled by the tunable splitting of the transverse electric and transverse magnetic optical modes, which is confirmed by both experiment and simulation. Based on the tunable effective magnetic field, the optical spin current can be controlled by the tunable cavity length in an open cavity. Our results will facilitate the development of optical spintronic devices and guide the understanding of analogies and generalizations involving quantum and classical wave theories.

DOI: [10.1103/PhysRevApplied.20.024028](https://doi.org/10.1103/PhysRevApplied.20.024028)

I. INTRODUCTION

Due to the relativistic spin-orbit coupling effect, carriers of different spins subject to impurity scattering form a spin flow, a phenomenon known as the spin Hall effect [1]. As relativistic spin-1 particles, photons naturally exhibit intrinsic spin-orbit interaction effects stemming from the fundamental spin properties of the Maxwell equations [2]. Therefore, analogues of the spin Hall effect can be found in various optical systems, such as a planar interface [3], metasurfaces with polarization-dependent phase manipulation [4–6], and waveguides with evanescent field tails [7–9]. The increasing researches on the optical spin Hall effect (OSHE) have also facilitated a series of applications [10] including precision metrology [11–14], analog optical computing [15–17], and quantum information technologies [18].

Among all the systems to investigate the OSHE, a microcavity consisting of two high-reflectance Bragg mirrors has drawn particular attention as it hosts massive photons with parabolic energy-momentum dispersion, light-matter coupling, as well as optical simulations [19–22]. The OSHE in a microcavity was initially predicted by Kavokin *et al.* [23], followed by experimental demonstrations in both strong coupling regime [24] and a bare microcavity [25–27]. Most recently, the increasing interest in optical analogues of condensed matter physics is intrigued by the interplay of the OSHE with unprecedented flexible tunability in optical systems. These tuning systems including birefringence, non-Hermitian effect, optical activity, and potential engineering, together with the intrinsic OSHE, have led to many hallmarks in optical simulations varying from polariton topological insulators [28,29] and skyrmions [30] to the photonic Rashba effect [31,32].

In electronic systems, it is known that both electrons and holes can experience spin-orbit coupling (SOC), and the direction of the effective magnetic field induced by the orbital movement will be reversed for electrons and holes. Furthermore, it has been shown that hole spins

*zhanglong@xmu.edu.cn

†zhanghai@xmu.edu.cn

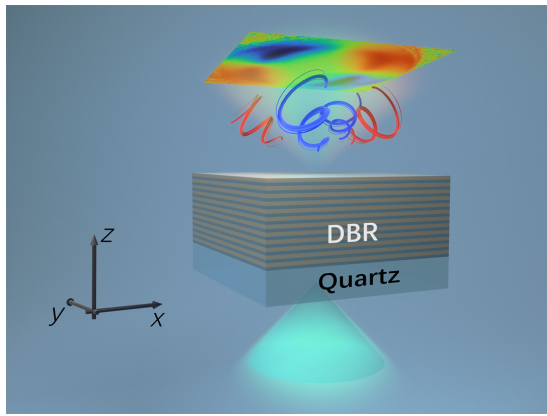


FIG. 1. Schematic of optical spin Hall effect in a one-dimensional photonic crystal.

in semiconductor nanostructures can experience a spin-orbit interaction many times stronger than that for electron spins, which has been revealed in the band structure of semiconductors [33–35].

However, this charge conjugation of SOC in optical systems has been absent as a result of the charge-free nature of photons. Moreover, the small strength of optical spin-orbit coupling is a major obstacle to extending the optical modeling of condensed matter physics and applications of optical spin devices [5,8].

In this paper, we revisit the OSHE in a one-dimensional photonic crystal (PC), also known as a distributed Bragg reflector (DBR), as schematically shown in Fig. 1. Taking advantage of the band structure of the photonic crystal and the large splitting between the transverse electric (TE) and transverse magnetic (TM) optical modes, we observe a reversible OSHE of photons from two edges of the photonic stop band, e.g., the direction of the optical spin current from the edge Bragg modes is opposite. Considering the similarity between the photonic stop band and electronic band gap, such a spin-band locking effect provides an optical analogue of the charge conjugation effect in an electron system. The experimental results agree well with numerical simulations. Based on this effect, we propose an electrically controlled open cavity to generate tunable optical spin current. Our results provide an understanding of the OSHE in photonic structures, and will pave a way to mimic spin-related condensed matter physics in optical systems.

II. BAND STRUCTURE AND TE-TM SPLITTING

The sample used in the experiment is a DBR mirror consisting of 12 pairs of low-index/high-index LiF/ZnS layers grown on a quartz substrate. The index of isotropic LiF and ZnS is about 1.39 and 2.35, respectively [36,37], and the high contrast of index will result in a larger TE-TM splitting and stronger OSHE, discussed in the following

sections. Both reflectance and transmission spectra of the structure can be obtained using spectroscopic measurements (see Fig. S1 within the Supplemental Material [38] for a schematic of the setup).

We first characterize the band structure of the PC by angle-resolved reflectance spectroscopy, as shown in Fig. 2(a). Determined by the optical length of each dielectric layer, the PC exhibits high reflectivity close to one in the spectral range from 2.0 to 2.5 eV. The broad high-reflectance region, also known as the optical stop band, is an optical analogue of the electronic band gap. The stop band is surrounded by optical modes with parabolic dispersion, called Bragg modes. The upper and lower branches of Bragg modes can be regarded as the optical conduction and valence bands of a PC, although there is no charge conjugation for photons. Each pair of Bragg modes is degenerate when the incident angle θ is zero. The degeneracy is lifted at finite incident angles, where the splitting increases proportionally to the incident angles. The origin of this splitting is confirmed by the polarization-resolved spectra, as shown in Figs. 2(b) and 2(c). Each pair of Bragg modes consists of a pair of TE and TM polarized modes with different dispersion, e.g., effective mass of photon. The band structure of the PC and polarization dependence can be well reproduced by simulation with the transfer matrix method (see Fig. S2 within the Supplemental Material [38] for the simulated results). This TE-TM splitting, resulting from the Fresnel law, plays a key role in the optical spin Hall effect, which has been explored in optical microcavities [23,26,27]. For a multiple layered optical structure with in-plane isotropy, the effective optical index to TE and TM polarized light will be different at nonzero incident angles, resulting in the lifted degeneracy of TE-TM mode. To investigate the TE-TM splitting quantitatively, we extract the energies of the first upper and lower Bragg modes at the edges of the photonic band gap, and plot them as a function of incident angle, as shown in Figs. 2(d) and 2(e), respectively. The TE and TM polarized modes are represented by the red solid and blue dashed lines, respectively. Interestingly, the TE polarized mode is energetically higher than the TM polarized mode for the upper Bragg mode, and the relationship is reversed for the lower Bragg mode. We define the TE-TM splitting as $\Delta = E_{\text{TE}} - E_{\text{TM}}$, which is positive for the upper Bragg modes and negative for the lower Bragg modes.

III. BAND EDGE DEPENDENCE OF OPTICAL SPIN HALL EFFECT

To illustrate the impact of TE-TM splitting on the optical spin Hall effect, the effective Hamiltonian of this system can be expressed in the form of a Pauli matrix [23]:

$$\hat{H}_k = \frac{\hbar^2 k^2}{2m} + \mu_B g (\boldsymbol{\sigma} \mathbf{H}_{\text{eff}}). \quad (1)$$

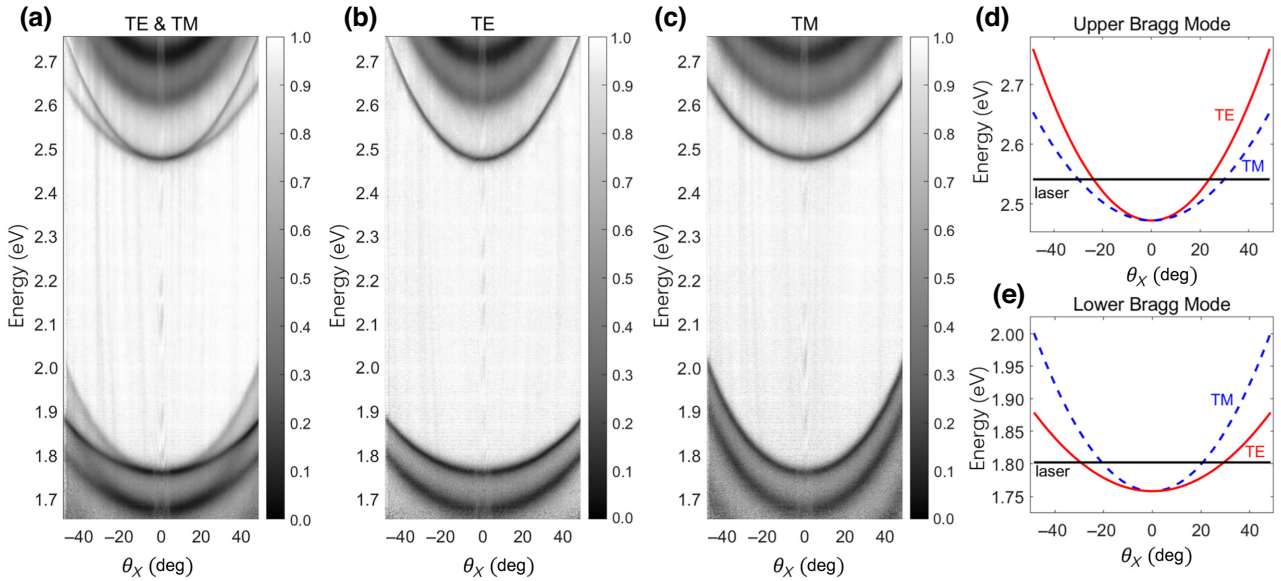


FIG. 2. Angle-resolved reflectance of the DBR. The measured reflectance (a) without polarization resolution, (b) with TE polarization, and (c) with TM polarization. The extracted dispersion of the (d) upper and (e) lower Bragg mode. The TE and TM components are plotted as red solid line and blue dashed line, respectively. The horizontal black solid line indicates the energy of the laser used for excitation.

The first term is the kinetic energy of the photon, where m is the effective mass with $m^{-1} = (m_{\text{TE}}^{-1} + m_{\text{TM}}^{-1})/2$. The second term is contributed by the TE-TM splitting, where σ is the Pauli matrix vector, μ_B is the Bohr magneton, and g is the g -factor. The TE-TM splitting results in an effective magnetic field $\mathbf{H}_{\text{eff}} = (\hbar/\mu_B g)\Omega_k$, and Ω_k can be further decomposed to

$$\Omega_x = \frac{\Delta(k_x^2 - k_y^2)}{\hbar k^2}, \quad \Omega_y = 2 \frac{\Delta(k_x k_y)}{\hbar k^2}. \quad (2)$$

Therefore, the orientation of the effective magnetic field acting on the cavity photons is determined by the in-plane momentum of photons, as indicated by the red arrows in Figs. 3(a) and 3(b), corresponding to the upper and lower Bragg modes, respectively. The opposite orientation of the magnetic field results from the opposite sign of TE-TM splitting of the two modes. In the presence of such effective magnetic field, the evolution of the circularly polarized light will be correlated with the in-plane wave vector. The procession of the photon under the anisotropic effective magnetic field in momentum space will result in anisotropic distribution of circularly polarized light. To map out this distribution and investigate its band structure dependence, a wavelength-tunable supercontinuum laser is used to excite the upper and lower Bragg modes separately. The energy of the excited photon is labeled by the horizontal black sold lines in Figs. 2(d) and 2(e), where the PC modes with finite in-plane wave vector exhibit nonzero TE-TM splitting. The incident light is linearly polarized, and focused by an objective with numerical aperture of

0.5. Photons with linear polarization will occupy the full momentum space by the resonant pump, as indicated by the blue arrows. The polarization will process under the effective magnetic field. We perform momentum space imaging of the degree of circular polarization (DOCP) defined as

$$\rho_c(k_x, k_y) = \frac{I_{\sigma-}(k_x, k_y) - I_{\sigma+}(k_x, k_y)}{I_{\sigma-}(k_x, k_y) + I_{\sigma+}(k_x, k_y)}, \quad (3)$$

where $I_{\sigma+}$ and $I_{\sigma-}$ represent the intensity of the transmitted light with right-circular polarization (RCP) and left-circular polarization (LCP). Figure 3 shows the experimental and simulated reciprocal space images of the DOCP for the upper and lower Bragg modes. For incident light with polarization along the y axis and with frequency on resonance with the upper Bragg mode [Fig. 3(c)], we observe a quadrupole of the DOCP with RCP and LCP symmetrically separated in different quadrants. In contrast, when the photon frequency is on resonance with the lower Bragg mode, the quadupole of the DOCP exhibits the opposite sign, as expected from the reversed orientation of the effective magnetic field. We perform simulation using the transfer matrix method followed by a coordinate transformation [26] (see Sec. C within the Supplemental Material [38] for details of this simulation method). The simulated patterns of DOCP agree well with the experiments, as shown in Figs. 3(e) and 3(f). We perform the same measurements and simulations when the incident light is polarized along the x axis, where the spin textures for the upper and lower Bragg modes exhibit a reversed

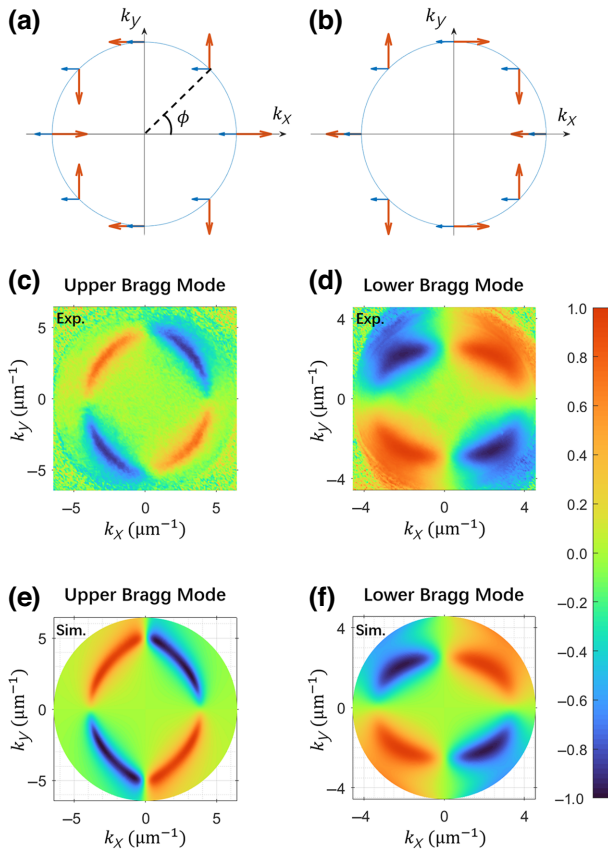


FIG. 3. Band edge dependence of the optical spin Hall effect. The effective magnetic field in momentum space for the (a) upper and (b) lower Bragg modes. The red arrows indicate the orientation of the effective magnetic field, and the shorter blue arrows indicate the initial direction of the pseudospin determined by the polarization of the pump. The polar angle is represented by ϕ . The measured spin textures [DOCP defined in Eq. (3)] of the (c) upper and (d) lower Bragg modes. The simulated results are plotted in (e),(f) correspondingly.

pattern [24] (see Fig. S3 within the Supplemental Material [38] for the measured and simulated results). Interestingly, the polarization patterns for the upper and lower Bragg mode are squeezed in x and y directions, respectively, which results from the TE-TM splitting of the mode as well (see Fig. S4 within the Supplemental Material [38] for a detailed discussion).

IV. TUNABLE OSHE IN AN OPEN CAVITY

To extend the tunability of the OSHE in the photonic structure, we explore the TE-TM splitting in a full cavity consisting of two DBRs. It has been shown that the cavity mode as an optical analogue of the defect state in electronic systems supports the OSHE as well [23]. As we sweep the length of the cavity, the mode will shift within the stop band [39]. To investigate the cavity length dependence of the TE-TM splitting, we simulate the polarization-resolved

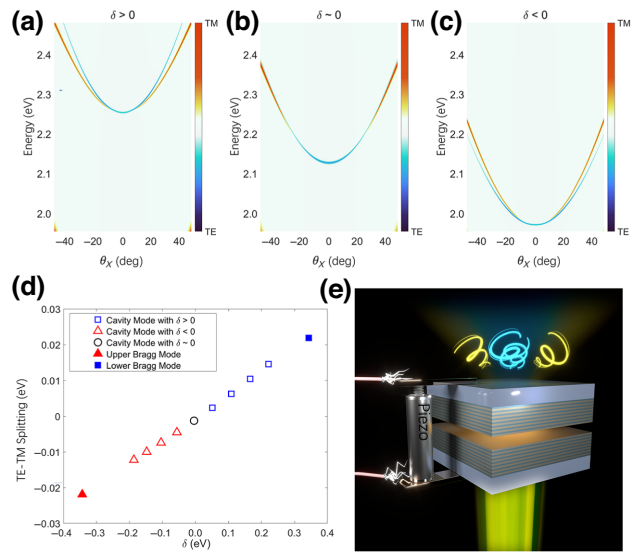


FIG. 4. Tunable TE-TM splitting in an open cavity. (a)–(c) The simulated angle-resolved reflectance for three different cavity lengths. The color of the mapping indicates the polarization, with red and blue corresponding to TM and TE polarization, respectively. We define detuning δ as the energy difference of the cavity mode compared with the center of the stop band. Three cases when (a) $\delta > 0$, (b) $\delta \sim 0$, and (c) $\delta < 0$. (d) Extracted TE-TM splitting at 20° with different detunings. The blue open square and the red open triangle represent the cavity modes with blue and red detuning, respectively. The blue filled square and the red filled triangle represent the upper and lower Bragg modes, respectively. The black open circle corresponds to the case of zero detuning. (e) Schematic of an optical spin current device that allows electrical control.

reflection spectra of a cavity corresponding to three different cavity lengths. As shown in Fig. 4(b), when the energy of the cavity mode (E_c) is exactly at the center of the stop band (E_0), the TE and TM modes overlap with each other. When the cavity mode is detuned from E_0 , the modes split in the opposite way, as indicated by Figs. 4(a) and 4(c). We define detuning as $\delta = E_c - E_0$. The amplitude of splitting extracted at a fixed angle (20°) will increase with the amplitude of δ , as shown by the open symbols in Fig. 4(d), where triangles and squares correspond to the negative and positive detunings (TE-TM splittings), respectively. As a reference, the dependence for the upper and lower Bragg modes is also plotted by filled symbols, which can be understood as the limit of the tunable cavity mode. Therefore, based on this detuning dependence of the effective magnetic field, we propose that an open cavity whose cavity length can be controlled continuously can support tunable OSHE. The open cavity has been widely applied in exploring solid-state light-matter interactions [40]. By tuning the cavity length through a piezo-controlled open cavity, both the orientation and size of the effective magnetic field can be controlled. Therefore the optical spin

current can be reversed by electrical control, which can be readily expected considering the mature open cavity techniques [40–43].

V. CONCLUSION

In conclusion, we report the band edge dependence of the optical spin Hall effect in a one-dimensional photonic crystal. The orientation of the optical spin current, determined by the direction of the effective magnetic field, exhibits strong correlation with the band structure. This is confirmed by the spin texture obtained experimentally, which is reproduced by simulation as well. Such a band-edge-related spin Hall effect provides an optical analogue of charge conjugation in spin-orbit interaction. By systematically investigating the mode dependence of the effective magnetic field, electrically tunable OSHE can be obtained in an open cavity. Our results contribute to the understanding of the optical analogue of the spin Hall effect and pave a way to improve its tunability. The Bragg modes with large TE-TM splitting can be readily coupled with van der Waals materials to investigate the optical spin Hall effect in the strong coupling regime [44]. The TE-TM splitting in an open cavity provides a tuning method for the OSHE, and facilitates its applications in optical simulation, topological photonics, and optical spin circuits.

ACKNOWLEDGMENTS

The work is supported by National Key R&D Program of China (Grants No. 2018YFA0306304), the National Natural Science Foundation of China (Grants No. 91950201, No. 62175207, and No. 92250301), Fundamental Research Funds for the Central Universities (20720210004), China Postdoctoral Science Foundation under Grant No. 2021M691890, and Natural Science Foundation of Fujian Province under Grant No. 2021J01007.

- [1] M. I. Dyakonov and V. I. Perel, Current-induced spin orientation of electrons in semiconductors, *Phys. Lett. A* **35**, 459 (1971).
- [2] K. Y. Bliokh, D. Smirnova, and F. Nori, Quantum spin Hall effect of light, *Science* **348**, 1448 (2015).
- [3] O. Hosten and P. Kwiat, Observation of the spin Hall effect of light via weak measurements, *Science* **319**, 787 (2008).
- [4] Y. Liu, Y. Ke, H. Luo, and S. Wen, Photonic spin Hall effect in metasurfaces: A brief review, *Nanophotonics* **6**, 51 (2017).
- [5] X. Yin, Z. Ye, J. Rho, Y. Wang, and X. Zhang, Photonic spin Hall effect at metasurfaces, *Science* **339**, 1405 (2013).
- [6] S. Luo, Z. Xu, L. Zhang, Z. Song, and Z. Chen, Convolution Operation on Pancharatnam-Berry Coding Metasurfaces in Visible Band, *Phys. Rev. Appl.* **19**, 054065 (2023).
- [7] L. Marrucci, Spin gives direction, *Nat. Phys.* **11**, 9 (2015).

- [8] K. Y. Bliokh, F. J. Rodríguez-Fortuño, F. Nori, and A. V. Zayats, Spin-orbit interactions of light, *Nat. Photonics* **9**, 796 (2015).
- [9] Z. Guo, H. Jiang, Y. Long, K. Yu, J. Ren, C. Xue, and H. Chen, Photonic spin Hall effect in waveguides composed of two types of single-negative metamaterials, *Sci. Rep.* **7**, 7742 (2017).
- [10] X. Ling, X. Zhou, K. Huang, Y. Liu, C.-W. Qiu, H. Luo, and S. Wen, Recent advances in the spin Hall effect of light, *Rep. Prog. Phys.* **80**, 066401 (2017).
- [11] X. Zhou, X. Ling, H. Luo, and S. Wen, Identifying graphene layers via spin Hall effect of light, *Appl. Phys. Lett.* **101**, 251602 (2012).
- [12] X. Zhou, L. Sheng, and X. Ling, Photonic spin Hall effect enabled refractive index sensor using weak measurements, *Sci. Rep.* **8**, 1221 (2018).
- [13] X. Zhou, Z. Xiao, H. Luo, and S. Wen, Experimental observation of the spin Hall effect of light on a nanometal film via weak measurements, *Phys. Rev. A* **85**, 043809 (2012).
- [14] X. Zhou, J. Zhang, X. Ling, S. Chen, H. Luo, and S. Wen, Photonic spin Hall effect in topological insulators, *Phys. Rev. A* **88**, 053840 (2013).
- [15] J. Zhou, H. Qian, C.-F. Chen, J. Zhao, G. Li, Q. Wu, H. Luo, S. Wen, and Z. Liu, Optical edge detection based on high-efficiency dielectric metasurface, *Proc. Natl. Acad. Sci. USA* **116**, 11137 (2019).
- [16] H. Kwon, D. Sounas, A. Cordaro, A. Polman, and A. Alù, Nonlocal Metasurfaces for Optical Signal Processing, *Phys. Rev. Lett.* **121**, 173004 (2018).
- [17] T. Zhu, Y. Lou, Y. Zhou, J. Zhang, J. Huang, Y. Li, H. Luo, S. Wen, S. Zhu, Q. Gong, M. Qiu, and Z. Ruan, Generalized Spatial Differentiation from the Spin Hall Effect of Light and Its Application in Image Processing of Edge Detection, *Phys. Rev. Appl.* **11**, 034043 (2019).
- [18] C. Chi, Q. Jiang, Z. Liu, L. Zheng, M. Jiang, H. Zhang, F. Lin, B. Shen, and Z. Fang, Selectively steering photon spin angular momentum via electron-induced optical spin Hall effect, *Sci. Adv.* **7**, eabf8011 (2021).
- [19] X. Liu, T. Galfsky, Z. Sun, F. Xia, E.-c. Lin, Y.-H. Lee, S. Kéna-Cohen, and V. M. Menon, Strong light-matter coupling in two-dimensional atomic crystals, *Nat. Photonics* **9**, 30 (2015).
- [20] J. Wang, R. Su, J. Xing, D. Bao, C. Diederichs, S. Liu, T. C. Liew, Z. Chen, and Q. Xiong, Room temperature coherently coupled exciton-polaritons in two-dimensional organic-inorganic perovskite, *ACS Nano* **12**, 8382 (2018).
- [21] Y. Sun, P. Wen, Y. Yoon, G. Liu, M. Steger, L. N. Pfeiffer, K. West, D. W. Snoke, and K. A. Nelson, Bose-Einstein Condensation of Long-Lifetime Polaritons in Thermal Equilibrium, *Phys. Rev. Lett.* **118**, 016602 (2017).
- [22] J. Zhao, R. Su, A. Fieramosca, W. Zhao, W. Du, X. Liu, C. Diederichs, D. Sanvitto, T. C. H. Liew, and Q. Xiong, Ultralow threshold polariton condensate in a monolayer semiconductor microcavity at room temperature, *Nano Lett.* **21**, 3331 (2021).
- [23] A. Kavokin, G. Malpuech, and M. Glazov, Optical Spin Hall Effect, *Phys. Rev. Lett.* **95**, 136601 (2005).
- [24] C. Leyder, M. Romanelli, J. P. Karr, E. Giacobino, T. C. H. Liew, M. M. Glazov, A. V. Kavokin, G. Malpuech, and A. Bramati, Observation of the optical spin Hall effect, *Nat. Phys.* **3**, 628 (2007).

- [25] A. Amo, T. C. H. Liew, C. Adrados, E. Giacobino, A. V. Kavokin, and A. Bramati, Anisotropic optical spin Hall effect in semiconductor microcavities, *Phys. Rev. B* **80**, 165325 (2009).
- [26] M. Maragkou, C. E. Richards, T. Ostatnický, A. J. D. Grundy, J. Zajac, M. Hugues, W. Langbein, and P. G. Lagoudakis, Optical analogue of the spin Hall effect in a photonic cavity, *Opt. Lett.* **36**, 1095 (2011).
- [27] K. Lekenta, M. Król, R. Mirek, K. Łempicka, D. Stephan, R. Mazur, P. Morawiak, P. Kula, W. Piecek, P. G. Lagoudakis, B. Piętka, and J. Szczytko, Tunable optical spin Hall effect in a liquid crystal microcavity, *Light Sci. Appl.* **7**, 74 (2018).
- [28] A. Nalitov, D. Solnyshkov, and G. Malpuech, Polariton Z Topological Insulator, *Phys. Rev. Lett.* **114**, 116401 (2015).
- [29] C. Li, F. Ye, X. Chen, Y. V. Kartashov, A. Ferrando, L. Torner, and D. V. Skryabin, Lieb polariton topological insulators, *Phys. Rev. B* **97**, 081103 (2018).
- [30] H. Flayac, D. D. Solnyshkov, I. A. Shelykh, and G. Malpuech, Transmutation from Skyrmions to Half-Solitons Driven by the Nonlinear Optical Spin-Hall Effect, *Phys. Rev. Lett.* **110**, 016404 (2013).
- [31] A. Nalitov, G. Malpuech, H. Terças, and D. Solnyshkov, Spin-Orbit Coupling and the Optical Spin Hall Effect in Photonic Graphene, *Phys. Rev. Lett.* **114**, 026803 (2015).
- [32] P. Kokhanchik, H. Sigurdsson, B. Piętka, J. Szczytko, and P. G. Lagoudakis, Photonic Berry curvature in double liquid crystal microcavities with broken inversion symmetry, *Phys. Rev. B* **103**, L081406 (2021).
- [33] D. V. Bulaev and D. Loss, Spin Relaxation and Decoherence of Holes in Quantum Dots, *Phys. Rev. Lett.* **95**, 076805 (2005).
- [34] D. V. Bulaev and D. Loss, Electric Dipole Spin Resonance for Heavy Holes in Quantum Dots, *Phys. Rev. Lett.* **98**, 097202 (2007).
- [35] F. N. M. Froning, M. J. Rančić, B. Hetényi, S. Bosco, M. K. Rehmann, A. Li, E. P. A. M. Bakkers, F. A. Zwanenburg, D. Loss, D. M. Zumbühl, and F. R. Braakman, Strong spin-orbit interaction and g-factor renormalization of hole spins in Ge/Si nanowire quantum dots, *Phys. Rev. Res.* **3**, 013081 (2021).
- [36] H. H. Li, Refractive index of alkali halides and its wavelength and temperature derivatives, *J. Phys. Chem. Ref. Data* **5**, 329 (1976).
- [37] M. Debenham, Refractive indices of zinc sulfide in the 0.405–13 μm wavelength range, *Appl. Opt.* **23**, 2238 (1984).
- [38] See Supplemental Material <http://link.aps.org/supplemental/10.1103/PhysRevApplied.20.024028> for details, which includes Refs. [23,24,26,36,37].
- [39] A. Kavokin, J. J. Baumberg, G. Malpuech, and F. P. Laussy, *Microcavities* (Oxford University Press, New York, 2007).
- [40] F. Li, Y. Li, Y. Cai, P. Li, H. Tang, and Y. Zhang, Tunable open-access microcavities for solid-state quantum photonics and polaritonics, *Adv. Quantum Tech.* **2**, 1900060 (2019).
- [41] T. Steinmetz, Y. Colombe, D. Hunger, T. W. Hänsch, A. Balocchi, R. J. Warburton, and J. Reichel, Stable fiber-based Fabry-Pérot cavity, *Appl. Phys. Lett.* **89**, 111110 (2006).
- [42] A. A. P. Trichet, P. R. Dolan, D. James, G. M. Hughes, C. Vallance, and J. M. Smith, Nanoparticle trapping and characterization using open microcavities, *Nano Lett.* **16**, 6172 (2016).
- [43] Y.-X. Zheng, J.-M. Cui, M.-Z. Ai, Z.-h. Qian, H. Cao, Y.-F. Huang, X.-J. Jia, C.-F. Li, and G.-C. Guo, Large-tuning-range frequency stabilization of an ultraviolet laser by an open-loop piezoelectric ceramic controlled Fabry-Pérot cavity, *Opt. Express* **29**, 24674 (2021).
- [44] X. Wang, L. Wu, X. Zhang, W. Yang, Z. Sun, J. Shang, W. Huang, and T. Yu, Observation of Bragg polaritons in monolayer tungsten disulphide, *Nano Res.* **15**, 1479 (2022).